Selected Paper

Single-Crystal Magnetic Study on Guest-Tunable Weak Ferromagnets [M{N(CN)$_2$}$_2$(pyrimidine)](guest) (M = Fe, Co)

Naomi Takagami,[1] Takayuki Ishida,*[1,2] and Takashi Nogami[1]

[1]Department of Applied Physics and Chemistry, The University of Electro-Communications, Chofu, Tokyo 182-8585

[2]Course of Coherent Optical Science, The University of Electro-Communications, Chofu, Tokyo 182-8585

Received November 19, 2003; E-mail: ishi@pc.uec.ac.jp

Low-temperature magnets derived from [M{N(CN)$_2$}$_2$(pm)] (M = Fe^{II}, Co^{II}) have guest molecules incorporated in the clearance of the three-dimensional framework, where pm stands for pyrimidine. A pm molecule in [Fe{N(CN)$_2$}$_2$(pm)](pm) (**1**) was characterized as a guest by means of X-ray crystallographic analysis. The guest molecules as well as the host N(CN)$_2$ skeletons are disordered in [Fe{N(CN)$_2$}$_2$(pm)](guest) (guest = EtOH (**2**), *n*-PrOH (**3**), 1/2 *n*-BuOH (**4**)) and also in [Co{N(CN)$_2$}$_2$(pm)](guest) (guest = EtOH (**5**), *n*-PrOH (**6**)). The ac and dc magnetic susceptibility measurements on randomly oriented polycrystalline samples of **1**–**6** revealed that they were weak ferromagnets (canted antiferromagnets) below T_N. The single-crystal magnetization measurements clarified the T_N's and the cant angles at 2 K as follows: $T_N = 5.6$ K, $\theta = 1.3°$ ($H \parallel c$) for **1**; $T_N = 3.3$ K, $\theta = 16°$ ($H \parallel c$) for **2**; $T_N =$ ca. 2 K, $\theta = 7.1°$ ($H \parallel b$) for **5**. The magnetic ground state seems to be related with single-ion anisotropy of the metal ions and the spin canting may take place as a combined result of the axial or in-plane anisotropy and antiferromagnetic interaction. The incorporated guest molecule tunes the single-ion anisotropy of the host metal ions, and consequently the magnetic phase transition phenomena were drastically different depending on the guest molecules.

There have been numerous reports on infinite metal–organic polymeric frameworks involving N-donor bridging ligands.[1] We have reported the magnetism of pyrimidine (pm)-bridged transition metal complexes in connection with the high-spin *m*-phenylene-bridged poly-carbenes and -radicals[2] and also the versatile utility of pm as a supramolecular synthon.[3] The role of pm as a magnetic coupler has been clarified to depend on the magnetic orbitals on the metal ions and the coordination geometries.[4,5] Various magnets have also been reported that contain d-transition metal ions and polycyano-anion bridges such as N(CN)$_2^-$.[6,7] Ternary systems attract much attention. Some peculiar crystal structures have been reported for [Mn{N(CN)$_2$}$_2$](pz)][8] and [Cu{N(CN)$_2$}$_2$(pz)],[9] where pz stands for pyrazine. We have already reported the transition metal complexes containing both pm and N(CN)$_2^-$ bridges, namely, [M^{II}\{N(CN)$_2$\}$_2$(pm)] (M = Fe,[10] Co,[10] Ni[11]) (Chart 1). Recently, we also developed the azide-bridged complexes, [M^{II}(N$_3$)$_2$(pm)] (M = Mn, Fe, Co, Ni), having a similar pillared-layer structure (Fig. 1) and a comparably higher T_N.[12] These metal dicyanamides and related ternary systems have often been characterized as canted antiferromagnets (weak ferromagnets),[6,7,10–13] and the origin of spin canting became of current interest.[14]

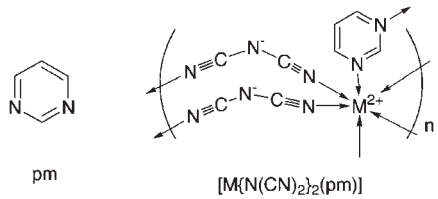

Chart 1.

Self-assembled complexes also attract attention for nano-porous materials that find potential applications in many areas (gas absorption for instance).[1] Porous magnets enable us to examine possible control of the magnetism by means of supramolecular techniques.[15] The specimen of [M{N(CN)$_2$}$_2$(pm)] prepared from an ethanol solution was revealed to contain ethanol molecules as a guest.[10] We have examined the solvent-dependence of the magnetic properties for the "solvated magnets" of [Fe{N(CN)$_2$}$_2$(pm)], since preparation from various solvents gave isomorphous compounds with only slight structural modification.[16] To investigate origins of the spin canting in [M{N(CN)$_2$}$_2$(pm)]-type compounds, we planned to study their single-crystal magnetic properties by varying the transition metal ions and guest molecules. Here we will concisely review the crystal structures of the host-guest compounds and the magnetic properties of randomly oriented polycrystalline sam-

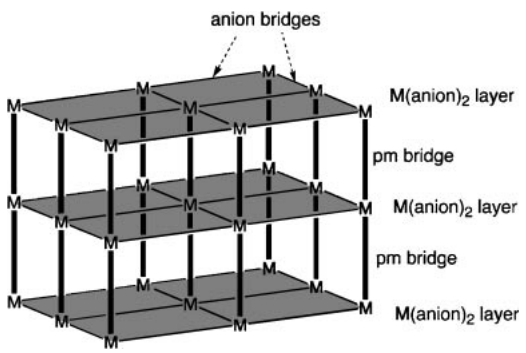

Fig. 1. Schematic drawing of the crystal structure of [M(X)$_2$(pm)] (M = Mn^{II}, Fe^{II}, Co^{II}, N^{II}; X = N(CN)$_2^-$, N$_3^-$).

Published on the web June 9, 2004; DOI 10.1246/bcsj.77.1125

ples for $[M\{N(CN)_2\}_2(pm)](guest)$.[10,11,16] A possible origin of the spin canting will be discussed after we describe the magnetic ordering phenomena on a single crystal of selected compounds.

Results

Crystal Structures. The X-ray crystal structure analysis reveals that the crystals of **1**–**6** are isomorphous, belonging to a space group orthorhombic *Pnma*. The cell parameters are summarized in Table 1, together with the composition determined from elemental analysis. Figures 2(a) and 2(b) show the ORTEP drawings of the $[Fe\{N(CN)_2\}_2(pm)]$ moiety in **1** as a host skeleton. There is only one Fe ion in an asymmetric unit. Each octahedral Fe ion resides at an inversion center and is coordinated by four nitrile N atoms at the equatorial sites and by two pm N atoms at the axial sites. The Fe^{II} and two $N(CN)_2^-$ ions construct a two-dimensional network parallel to the *ac* plane (Fig. 2(a)). The pm molecules bridge inter-sheet Fe ions along

Table 1. Cell Parameters of $[M\{N(CN)_2\}_2(pm)](guest)$ (**1**–**6**)[a)]

Compound	**1**	**2**	**3**	**4**	**5**	**6**[b)]
M	Fe	Fe	Fe	Fe	Co	Co
guest	pyrimidine	ethanol[c)]	propanol[c)]	1/2 butanol[c)]	ethanol[c)]	propanol[c)]
a/Å	13.0061(5)	12.917(1)	12.597(5)	12.9486(7)	12.8586(4)	12.768(3)
b/Å	12.3550(4)	12.0440(6)	12.001(6)	12.2052(6)	11.9268(4)	12.121(2)
c/Å	9.2235(4)	9.2575(8)	9.461(4)	9.4499(6)	9.2126(2)	9.292(2)
V/Å^3	1482.1(1)	1440.2(2)	1430(1)	1493.5(2)	1412.86(7)	1438.1(9)
D_{calcd}/g cm^{-3}	1.560	1.449	1.523	1.584	1.491	1.530
T/K	90	100	90	90	100	90

a) The space groups are orthorhombic *Pnma* with $Z = 4$ unless otherwise noted. Pm stands for pyrimidine.
b) Only the cell parameters were determined. c) Determined by elemental analysis (C, H, N).

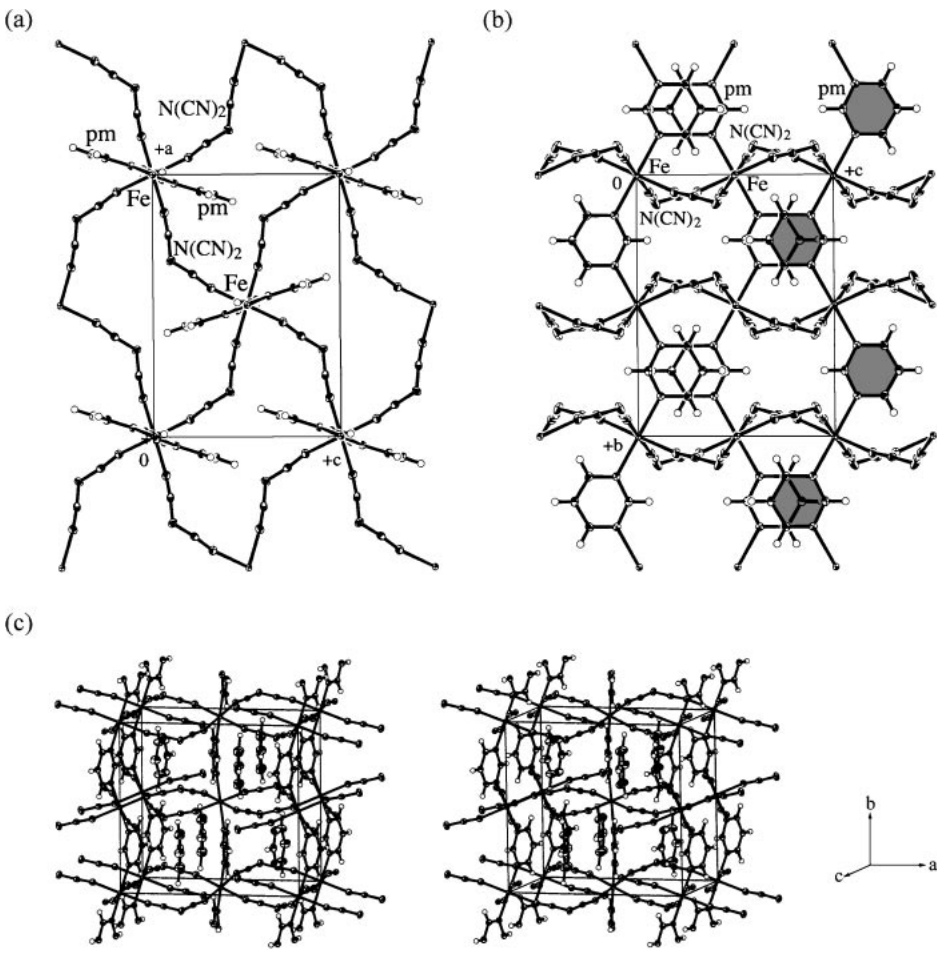

Fig. 2. (a,b) ORTEP drawings of $[Fe\{N(CN)_2\}_2(pm)](pm)$ (**1**), viewed along the *b* axis (a) and *a* axis (b). Thermal ellipsoids are drawn at the 50% probability level for non-hydrogen atoms. The guest pyrimidine molecules are omitted for the sake of clarity. A one-dimensional Fe–pm chain is shaded in (b). (c) A stereo-view of the crystal structure of **1**. Pm stands for pyrimidine.

the *b* axis to form a *trans* zigzag Fe–pm chain, as indicated by the shaded pm rings in Fig. 2(b). Thus, the $N(CN)_2^-$ and pm moieties contribute μ-1,5-bridged two-dimensional and μ-1,3-bridged one-dimensional structures, respectively, constructing a three-dimensional framework (Fig. 1).

Important geometries are described for **1**. Four nitrile nitrogen atoms are coordinated at the equatorial sites with the Fe–$N_{nitrile}$ distances of 2.126(1) and 2.141(1) Å, and by two pm nitrogen atoms at the axial sites with the Fe–N_{pm} distance of 2.219(1) Å. The $N_{nitrile}$–Fe–N_{pm} angles range from 88.87(5) to 91.13(5)°. The amide nitrogen atom does not participate in coordination. The central C–N–C angle is 120.3(1)°, the N–C≡N angles are 173.4(2) and 173.7(2)°, and the C≡N–Fe angles are 163.6(1) and 167.1(1)°. The Fe···Fe separation of 6.1775(2) Å across the pm bridge is shorter than the intra-sheet Fe···Fe separation of 7.9723(2) Å across the $N(CN)_2^-$ bridge, and accordingly the pm bridge may afford a principal magnetic exchange pathway. Owing to the strong directionality of the pm lone-pairs, the elongated octahedral axes of neighboring Fe ions are relatively inclined by 118°.

The guest molecule in **1** was characterized to be an uncoordinated pm (Fig. 2(c)). The hydrogen atoms in the guest pm were experimentally found and the positional parameters were optimized successfully. The analysis revealed no disorder of the nitrogen position. Although the *R* factors in the refinement were satisfactorily lowered, thermal ellipsoids in the guest pm are somewhat larger, even at 90 K, than those in the host. The site occupancy of the guest pm was refined to be almost unity, in good agreement of the elemental analysis.

The $[Fe\{N(CN)_2\}_2(pm)]$ skeletons are essentially the same among **1**–**4**, except for the small change of the cell lengths (Table 1). The solvent molecules in **2**–**4** were found in difference Fourier maps but their positional and thermal displacement parameters could not be completely determined owing to disorder. In addition to the guest disorder, the skeletal $N(CN)_2^-$ bridges in **2**–**4** also showed disorder. The detailed crystal structure of **2** measured at 100 K was published elsewhere.[10] The equatorial Fe–$N_{nitrile}$ distances are 2.138(4) and 2.142(4) Å, and the axial Fe–N_{pm} distance is 2.202(4) Å. The $N_{nitrile}$–Fe–N_{pm} angles range from 89.6(2) to 90.4(2)°. The intra- and inter-sheet Fe···Fe separations are 7.9458(5) and 6.0220(3), respectively.

The crystal structure of **5** is also isomorphous to that of **2**.[10] The guest ethanol molecules and the host $N(CN)_2^-$ bridges are disordered. The Co–$N_{nitrile}$ bond lengths are 2.103(4) and 2.105(4) Å and the Co–N_{pm} bond length 2.154(4) Å. The slightly elongated octahedron was characterized with the pm nitrogen atoms at the axial positions, in the same way as **1** and **2**. The intra- and inter-sheet Co···Co separations are 7.9091(2) and 5.9634(2), respectively. The metal–nitrogen bond lengths for **1**, **2**, and **5** are summarized in Table 2. The Co–N bond lengths are shorter than the Fe–N bond lengths in an isomorphous series,[5] and accordingly the cell volume of **5** is smaller than that of **2**.

Magnetic Properties for Polycrystalline Samples. We measured field-cooled magnetization (FCM), remnant magnetization (RM), and zero-field-cooled magnetization (ZFCM) of randomly oriented polycrystalline specimens of **1**–**4**. The temperature dependence of the FCMs at 5 Oe showed clear upsurges at about 5.6, 3.7, 4.6, and 3.6 K for **1**–**4**, respectively, and, after the applied field was removed, the RMs disappeared at the same temperatures. The FCM results are summarized in Fig. 3(a). We measured the ac magnetic susceptibility (Figs. 3(b) and 3(c); χ_{ac}' and χ_{ac}'' for the real and imaginary parts, respectively) of **1**–**4**. As Fig. 3(b) shows, the χ_{ac}' measurements (100 Hz) exhibited peaks at 5.6, 3.3, 4.4, and 3.6 K, respectively, supporting the occurrence of the magnetic phase transition. We found no frequency dependence of T_N.

Table 2. The Metal–Nitrogen Bond Lengths (Å) of $[M\{N(CN)_2\}_2(pm)](guest)$ (**1**, **2**, and **5**)

Compound	**1**	**2**	**5**
M	Fe	Fe	Co
guest	pyrimidine	ethanol	ethanol
M–$N_{nitrile}$	2.126(1)	2.138(4)	2.103(4)
	2.141(1)	2.142(4)	2.105(4)
M–N_{pm}	2.219(1)	2.202(4)	2.154(4)

In order to clarify the nature of magnetism below T_N, we measured *M*–*H* curves at 2.0 K for the polycrystals of **1**–**4**. As reported in the previous communication,[10] the Fe^{II} ion in **2** has a high-spin state ($S = 2$) and dominant antiferromagntic interactions were clarified with a negative Weiss temperature (−7.0 K) in the paramagnetic phase. Figure 4 shows that **1**–**4** behave as weak ferromagnets, as indicated by spontaneous magnetizations (M_S) in a low field region. Stepwise saturation behavior was observed, the origin of which can be proposed as spin-flip transition from a canted antiferromagnetic phase to a canted ferromagnetic phase. The smaller M_S implies a smaller cant angle in a canted antiferromagnetic phase, and after a possible spin-flip transition the saturation magnetization should be larger in a canted ferromagnetic phase. This interpretation is supported by comparison of the *M*–*H* curve of **1** with those of **2**–**4**. The M_S of **1** was the smallest and the strong antiferromagnetic nature seems responsible for the small χ_{ac}' and χ_{ac}'' peaks of **1**. The M_S's at 2.0 K were found to be 0.2×10^3 and 5.8×10^3 erg Oe^{-1} mol^{-1} for **1** and **2**, respectively, indicating that the cant angles for **1** and **2** are 0.6 and 14° at the ground state. The coercive fields were <20 Oe, indicating a soft character of **1**–**4**. Small hysteresis-like behavior was found during the metamagnetic transition, but it is not intrinsic because the single-crystal magnetic study exhibited no hysteresis behavior (see below).

The magnetic properties of **5** have been described elsewhere.[10] The antiferromagnetic interactions among the high-spin Co^{II} ions ($S = 3/2$) were characterized for **5** with a negative Weiss temperature of −4.4 K.[10] The magnetization curve measured at 2.0 K showed an M_S of 2.5×10^3 erg Oe^{-1} mol^{-1} (Fig. 5(a)), indicating the cant angle of 7°. The coercive field was <20 Oe. The transition temperature was near 2.0 K, as determined by the FCM, RM, and ZFCM measurements together with the χ_{ac}' and χ_{ac}'' measurements. The $[Co\{N(CN)_2\}_2(pm)](guest)$ series also exhibited guest dependence of the magnetic phase transition phenomena. Actually, the sample prepared from propanol (**6**) showed the *M*–*H* curve with a more distinguished metamagnetic transition than that for **5** (Fig. 5(b)). The M_S of **6** at 2.0 K was almost the same as that of **5**. The transition temperature of **6** was 2.1 K, as determined by the FCM, RM, ZFCM, and ac susceptibility measurements.

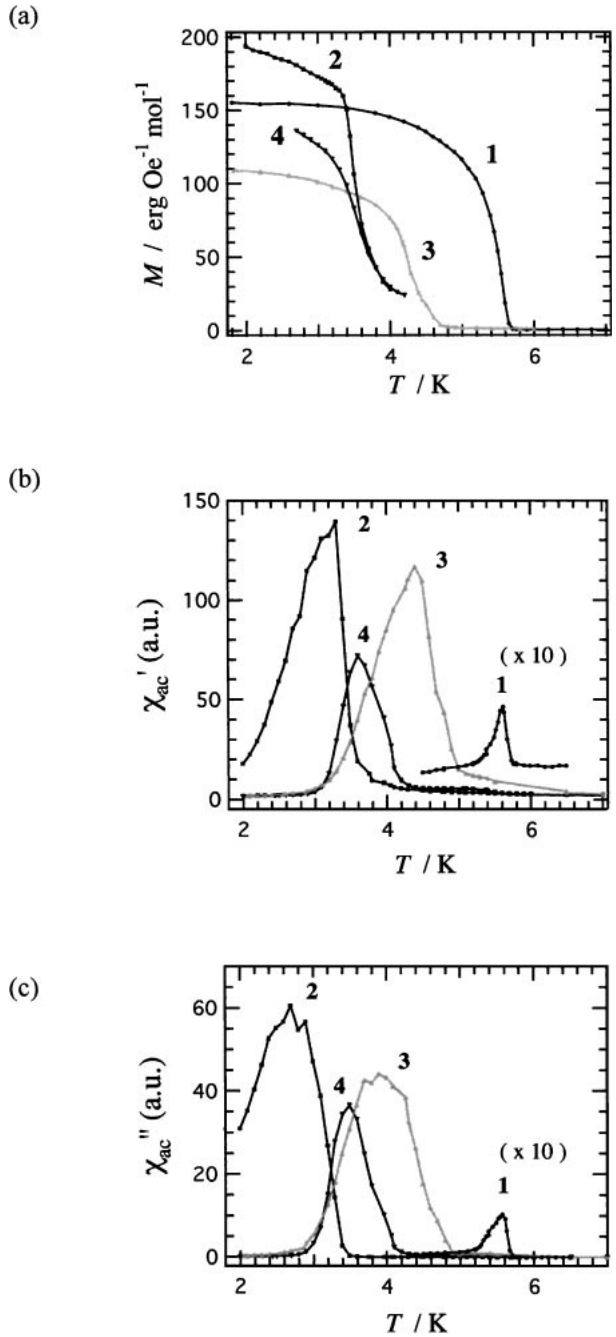

Fig. 3. (a) Field-cooled magnetization of **1**–**4** measured at 5 Oe. (b,c) Temperature dependence of χ_{ac}' (b) and χ_{ac}'' (c) for **1**–**4** ($\nu = 100$ Hz). Comparison of relative intensity is valid in the arbitrary scale.

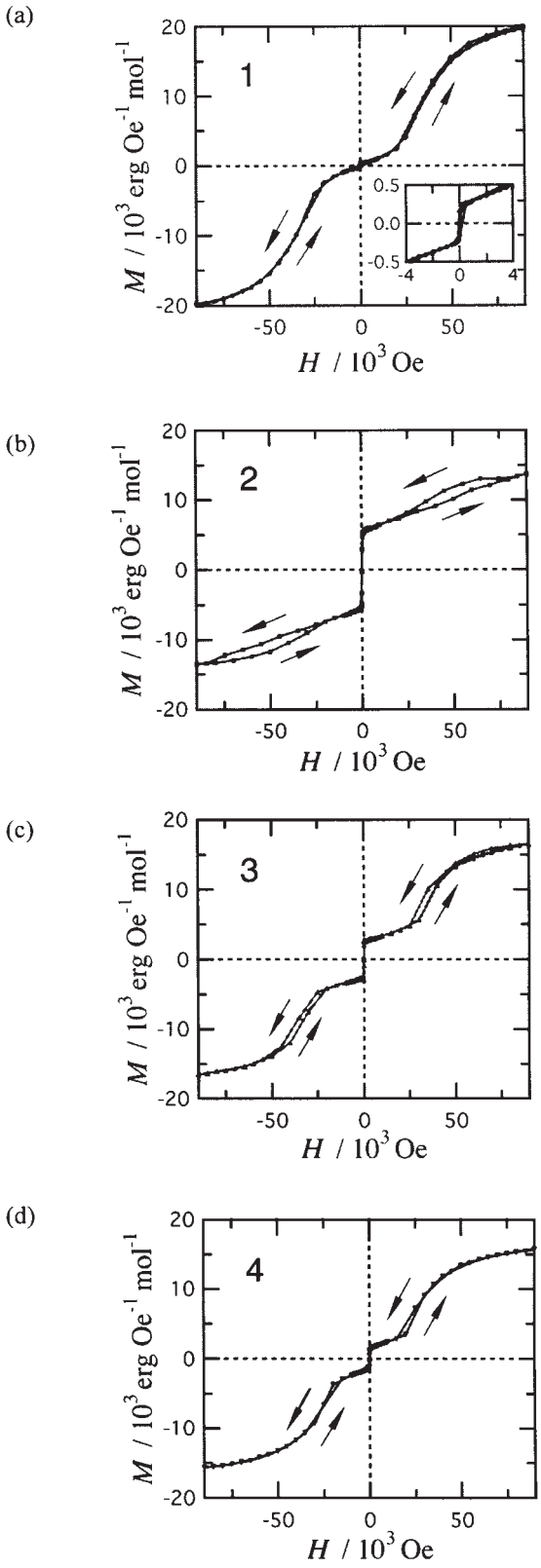

Fig. 4. (a–d) *M*–*H* curves of **1**–**4** measured at 2.0 K. Solid lines are shown for a guide to the eye.

However, the Co series is supposed to be rather inadequate for the detailed study of the guest dependence because the T_N's were too low for us to measure their magnetic properties precisely on our apparatus.

Magnetic Properties for Single-Crystal Samples. We measured FCM, RM, and ZFCM of a single crystal of **1**. As Fig. 6(a) shows, only when an external field was applied parallel to the crystallographic *c* axis did the magnetization show an obvious upsurge near T_N (5.6 K) upon cooling. The estimated mass of the single crystal specimen was 0.0475 mg. A rather large magnetic field (500 Oe) was applied because sufficient SQUID responses were recorded for the small crystal. Some biases were found for the data measured at the applied field par-

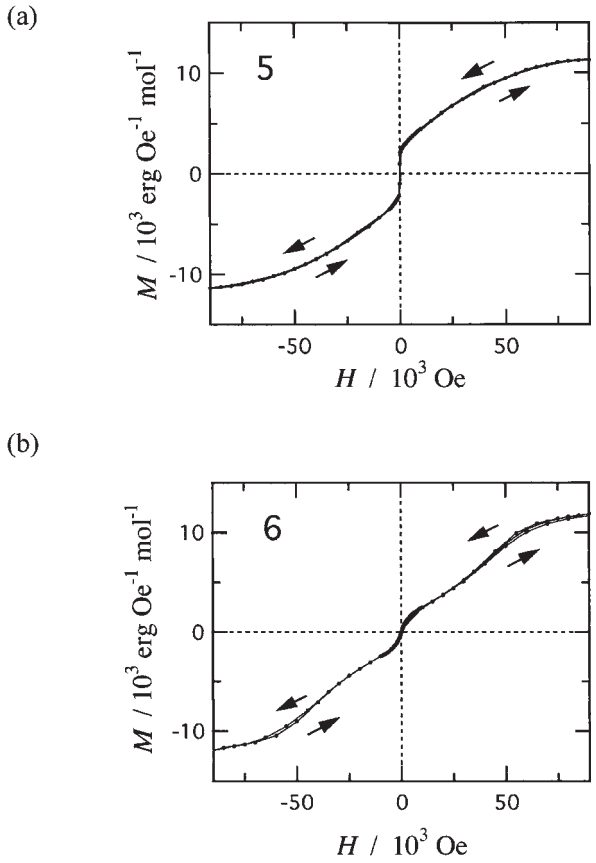

Fig. 5. (a,b) *M–H* curves of **5** and **6** measured at 2.0 K. Solid lines are shown for a guide to the eye.

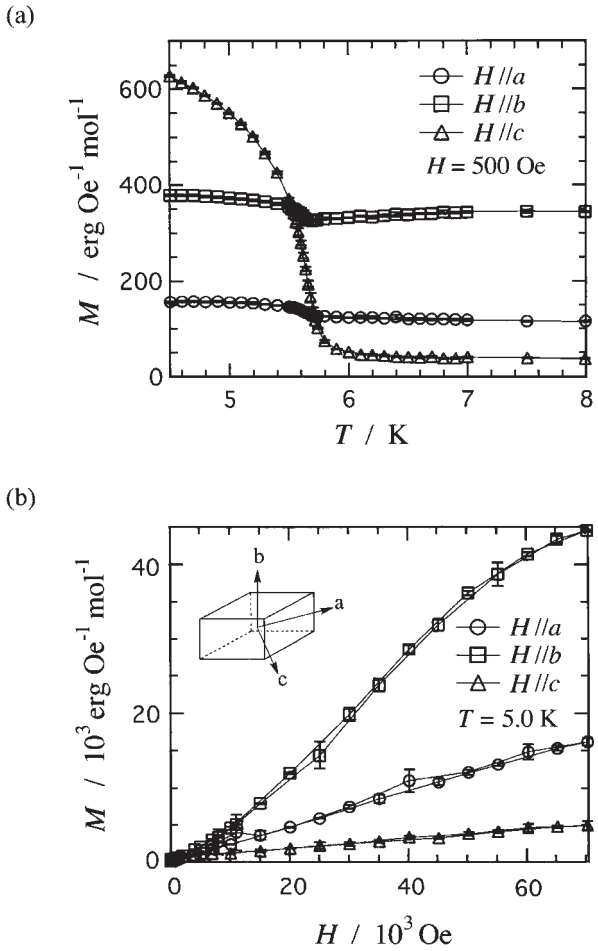

Fig. 6. (a) Field-cooled magnetization measurements of a single crystal of **1** with the applied fields of 500 Oe parallel to the *a*, *b*, and *c* axes. (b) Magnetization curves of **1** at 5 K with the applied field parallel to the *a*, *b*, and *c* axes. Solid lines are shown for a guide to the eye. Inset depicts the relation between the crystal habit and axis directions.

allel to the *b* and *a* axes and these are not essential; the magnetization upsurge is very small so that these biases seemed relatively large. Small kinks are found in the data measured with $H \parallel a$ and $H \parallel b$ but these are negligible within experimental error since the crystal was mounted manually under a microscope.

One may wonder whether the small ferromagnetic component observed for the polycrystalline samples is intrinsic in the crystal structure, especially for **1** showing the extremely small spontaneous magnetization (M_S). If we argue from the above results, however, the highly anisotropic FCM upsurge observed can be attributed genuinely to the crystal of **1** and not to impurities that contaminate.

This experiment clearly tells us that the spin canting direction is the *c* axis, and the magnetic easy axis is expected to reside perpendicular to that axis. We measured the precise angular dependence of FCM as a function of a rotation angle within the *ac* and *bc* planes. We found that they showed monotonic behavior and that the maximum and minimum were located just at the axis directions.

Figure 6(b) shows the *M–H* curves for **1** with the applied fields parallel to the *a*, *b*, and *c* axes. The magnetization along the *c* axis was the most insensitive to the applied field. This finding indicates that the magnetically hard axis should be assigned to the *c* axis, in good agreement of the canting direction determined from the FCM results. We can find an S-shaped magnetization curve in the data of $H \parallel b$. Therefore the magnetic structure of **1** at the ground state was described as a dominantly antiferromagnetic structure along the *b* axis with a small spin canting toward the *c* direction. The anisotropic bulk magnetism with respect to the magnetic unique *b* axis may be related to the Ising (S_z) spin character of the Fe^{II} ion (see Discussion section). The angle of spin canting was estimated to be 1.3° toward the *c* axis from the basal alignment on the *b* axis.

We similarly measured anisotropic properties in the FCM and *M–H* curves for **2**. Interestingly, the angular dependence of **2** was quite different from that of **1** despite the isomorphous crystals with the same metal ions. Figure 7(a) shows the FCM results on **2** at 500 Oe when the magnetic fields were applied along the *a*, *b*, and *c* axes. The magnetization due to spin canting was observed for the measurement with $H \parallel c$ just like **1**, and also relatively small magnetization for the measurement with $H \parallel b$. Practically no magnetization was observed in the measurement with $H \parallel a$. Figure 7(b) shows the *M–H* curves for **2** with the applied fields parallel to the *a*, *b*, and *c* axes. An M_S was clearly observed in the data of $H \parallel c$, and the data of $H \parallel a$ traced an S-shaped curve typical of metamagnetic behavior, obviously indicating that the *a* and *c* axes can be defined

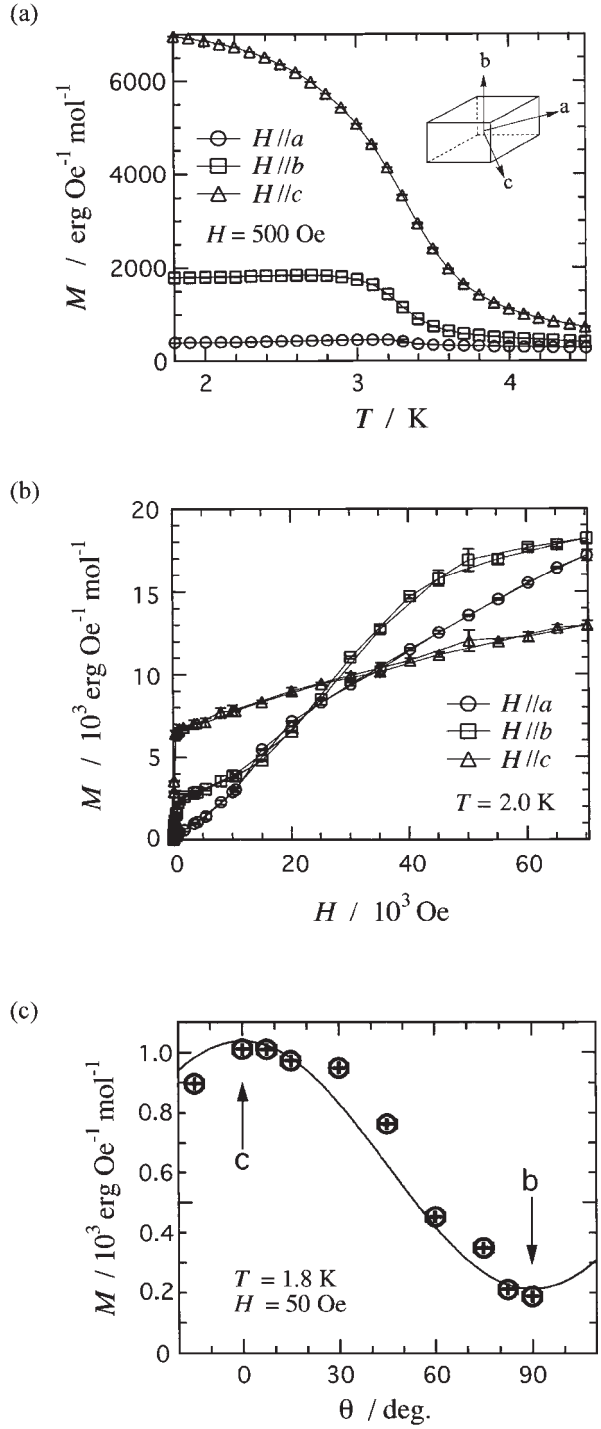

Fig. 7. (a) Field-cooled magnetization measurements of a single crystal of **2** with the applied fields of 500 Oe parallel to the *a*, *b*, and *c* axes. (b) Magnetization curves of **2** at 2.0 K with the applied fields parallel to the *a*, *b*, and *c* axes. (c) Angle dependence of the field-cooled magnetization of **2** at 1.8 K. Solid lines are shown for a guide to the eye.

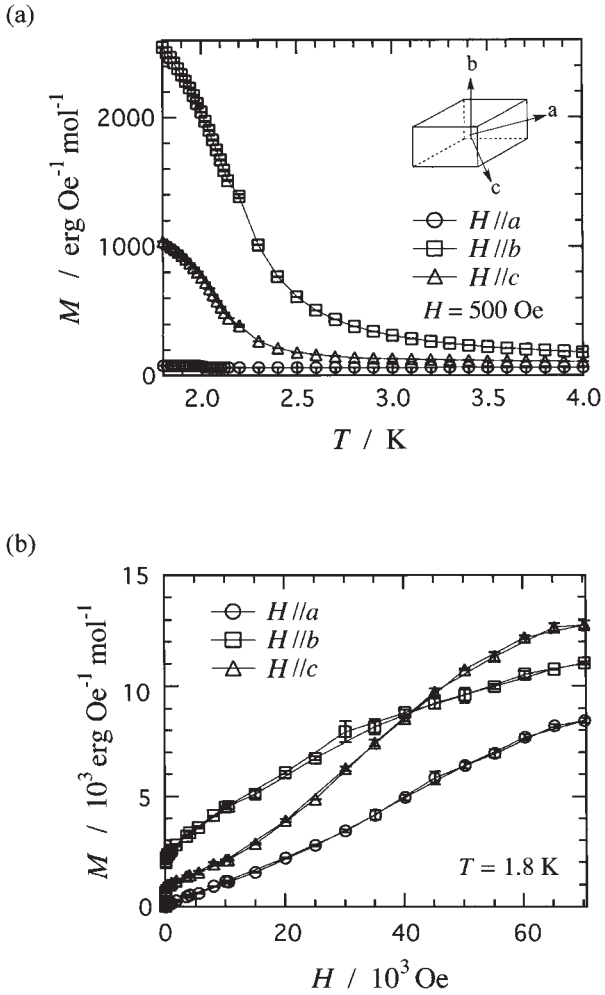

Fig. 8. (a) Field-cooled magnetization measurements of a single crystal of **5** with the applied fields of 500 Oe parallel to the *a*, *b*, and *c* axes. (b) Magnetization curves of **5** at 2.0 K with the applied fields parallel to the *a*, *b*, and *c* axes. Solid lines are shown for a guide to the eye.

as magnetically easy and hard axes, respectively. On the other hand, the data on $H \parallel b$ shows both features; i.e., the presence of M_S near 0 Oe and an S-shaped transition around 30 kOe. In general, M_S due to the spin canting should be observed in the perpendicular direction of dominant anitferromagnetic moments, but such a simple scheme can not explain the behavior of $H \parallel b$.

To clarify the magnetic structure when a magnetic field is applied along the *b* axis, we measured the angular dependence of FCM of **2**. Figure 7(c) shows the plot of the magnetization after a field-cooled process from 4.5 to 1.8 K at 50 Oe for each angle measurement. The *c* axis direction shows a maximum of magnetization and the *b* axis direction a minimum. The observed magnetization was substantial even at the minimum (parallel to the *b* axis) in the *bc* plane. Since the magnetization minima were assigned to be the *a* axis in both *ab* plane and *ac* plane, appreciable magnetization was present in any direction within the *bc* plane. This finding suggests an S_{xy} character of Fe^{II} spins in **2** (see Discussion section). Assuming that the spin is canted toward the *c* axis direction, one can estimate the cant angle to be 16°.

We investigated the FCM and *M*–*H* curves of a single crystal of **5**, which contain cobalt(II) ions in place of iron(II) ions of **2** in an isostructural crystal. Figure 8(a) shows the FCM results on **5** at 500 Oe. The magnetizations due to spin canting were

observed for the data on the *b* and *c* axes, and no magnetization was observed for the data on the *a* axis. It should be noted that the largest magnetization was found for the data in $H \parallel b$ for **5**, in sharp contrast to the largest magnetization in $H \parallel c$ for **2**. Figure 8(b) shows the *M*–*H* curves for **5**. M_S's were observed in the *b* and *c* axis directions and S-shaped magnetization curves were obtained along the *a* and *c* axes. Thus, the *a* and *b* axes can be defined as magnetically easy and hard axes, respectively. Anomalous behavior of $H \parallel c$ showing both M_S and metamagnetic behavior are found for **5**, like $H \parallel b$ in **2**, but the roles of the *b* and *c* axes are exchanged between **2** and **5**. The cant angle was estimated as 7.1° from the data of $H \parallel b$.

Discussion

We have found that the magnetic phase transition phenomena of **1**–**4**, such as the transition temperatures (T_N), metamagnetic transition critical fields, and the spontaneous magnetizations (M_S) (which correlate to the cant angles of spins), depend on the guest molecules from the experimental results on **1**–**4**. Actually, the T_N's of **1** and **2** were determined to be 5.6 and 3.3 K, respectively. The T_N difference of 2.3 K is relatively large in a liquid He temperature region. The magnetic properties are ascribed only to the host of the $[M\{N(CN)_2\}_2(pm)]$ skeleton, but the guest molecule affects the structure of the host. The coordination geometries around the metal ions are most likely deformed by the strain of the host through van der Waals repulsive or attractive interactions between the host and guests. The presence of the van der Waals interactions is supported by the disorder of the host $N(CN)_2$ skeletons in the compounds that include alcohol and by orderly arranged pm in **1**. This deformation may give rise to changes of single-ion properties (see below) as well as changes of the magnitude of spin–spin exchange coupling.

The present compounds $[M\{N(CN)_2\}_2(pm)](guest)$ are weak ferromagnets with a low coercive field and a very large ferromagnetic component (spontaneous magnetization) corresponding to a cant angle of up to 16° for **2**. This is one of the largest values reported. Such a large spin canting has been observed and well discussed for the non-centrosymmetric crystals such as $[MCl_2(pm)_2]$ (M = Fe,[17] Co[18]) and $[Fe(N_3)_2(bpy)]$ (bpy = 4,4′-bipyridyl).[19] However, the present compounds belong to a centrosymmetric *Pnma* space group. The magnetic structure might be acentric as a sublattice. Now we discuss possible origins of the spin cantings and ground spin structures in **1**, **2**, and **5** which significantly differs from each other. The difference between **1** and **2** is interesting in particular because **1** and **2** are isomorphous with the same metal ions. As described above, their single-crystal magnetic study revealed that the magnetic structures of the ground state were essentially different.

As for **1**, the anisotropy of the FCM and *M*–*H* curves may be basically interpreted in terms of the single-ion anisotropy. If we assume that Fe^{II} ions in **1** have an axial anisotropy, i.e., that the effective zero-field splitting (*D*) is negative, the moment on Fe^{II} tends to turn in the axial direction. We use the *D* parameter for convenience in discussion, though it is not accurately defined for iron(II) ions. The axial anisotropy is suggested for the canted antiferromagnet $[FeCl_2(pm)_2]$[17] and for other Fe^{II} coordination compounds.[20]

The X-ray crystallographic study indicates that the Fe^{II} ion has an elongated octahedron and that the pm nitrogen atoms are coordinated at the axial positions (Table 2). The pm bridge works as an antiferromagnetic coupler when pm nitrogen atoms are coordinated to form σ-type orbital overlaps between the metal e_g orbitals and nitrogen n orbital on both sides, leading to an antiferromagnetic superexchange through the pm molecular orbitals.[5] This interaction favors the antiparallel spin alignment between the neighboring spins. On the other hand, the pm has a rigid direction of 120° between two lone pairs and accordingly the axial anisotropy favors a 120° alignment across the pm bridge (Fig. 9(a)). As a consequence, from a balance of two contributions, $J < 0$ and $D < 0$, the spin is canted with an angle between 0 and 60°. As Fig. 2(b) shows, the pm–Fe zigzag chain is located almost on the *bc* plane, and the axial direction is nearer the *b* axis than the *c* axis. Therefore, this interpretation is consistent with the observed magnetic anisotropy; the dominant antiferromagnetic structure is defined to be the *b* axis and the spin canting direction is the *c* axis.

Table 2 shows slight changes of the metal–nitrogen bonds between **1** and **2**. In **2**, one of the equatorial Fe–$N_{nitrile}$ bonds is longer, while the axial Fe–N_{pm} bond is shorter, than those in **1**. The single-ion anisotropy of Fe^{II} may be changed by the geometrical changes around the Fe^{II} coordination sphere. The experimental results on **2** and **5** indicate that the moment can easily rotate depending on the direction of the applied magnetic field. This finding suggests the xy-character of the spin, i.e., the metal spin has an in-plane anisotropy (effectively $D > 0$) in **2** and **5**.

The spin of Co^{II} in **5** favors residing at the equatorial plane as depicted in Fig. 9(b). When an external magnetic field was applied parallel to the *a* axis, the moment can rotate and form an antiparallel alignment in the $\pm a$ directions. This situation fully satisfies the requirement, $J < 0$ and $D > 0$, and accordingly **5** behaves as a genuine antiferromagnet along the *a* axis. When an external field was applied in the *b* direction, the antiferromagnetic structure is ruled by a competition between $J < 0$ and $D > 0$. In a low field region, the antiferromagnetic structure is formed along the *a* axis, and the residual moment due to the spin canting can be observed in both *b* and *c* directions. On the other hand, with an increase of the applied field, the spin can rotate in an equatorial plane. The antiferromagnetic interaction favors the 180° alignment, but the in-plane anisotropy allows the 120° alignment. The cant angle becomes between 0° and 60°. This situation was observed as the principal antiferromagnetic structure along the *c* axis with the spin canting toward the *b* axis. Actually the experimental results on **5** can be explained by the above argument. The in-plane anisotropy of the Co^{II} ion has been discussed recently.[21]

The S_{xy}-characters were found in **2** and **5** but the roles of the *b* and *c* axes are changed. The reason is not clear so far. The *a* axis is unique and the *b* and *c* axis characters are similar to each other for **2** and **5**. Both **2** and **5** have the severe disorder of $N(CN)_2$ bridges,[10] which brings about a further deformation of the metal coordination sphere. The degree of the disorder may affect the magnitude and direction of in-plane anisotropy in **2** and **5**. One possibility is that the in-plane anisotropy of Fe^{II} ions in **2** is not located in the equatorial plane defined by the crystallographic bond lengths. Nevertheless, the experimen-

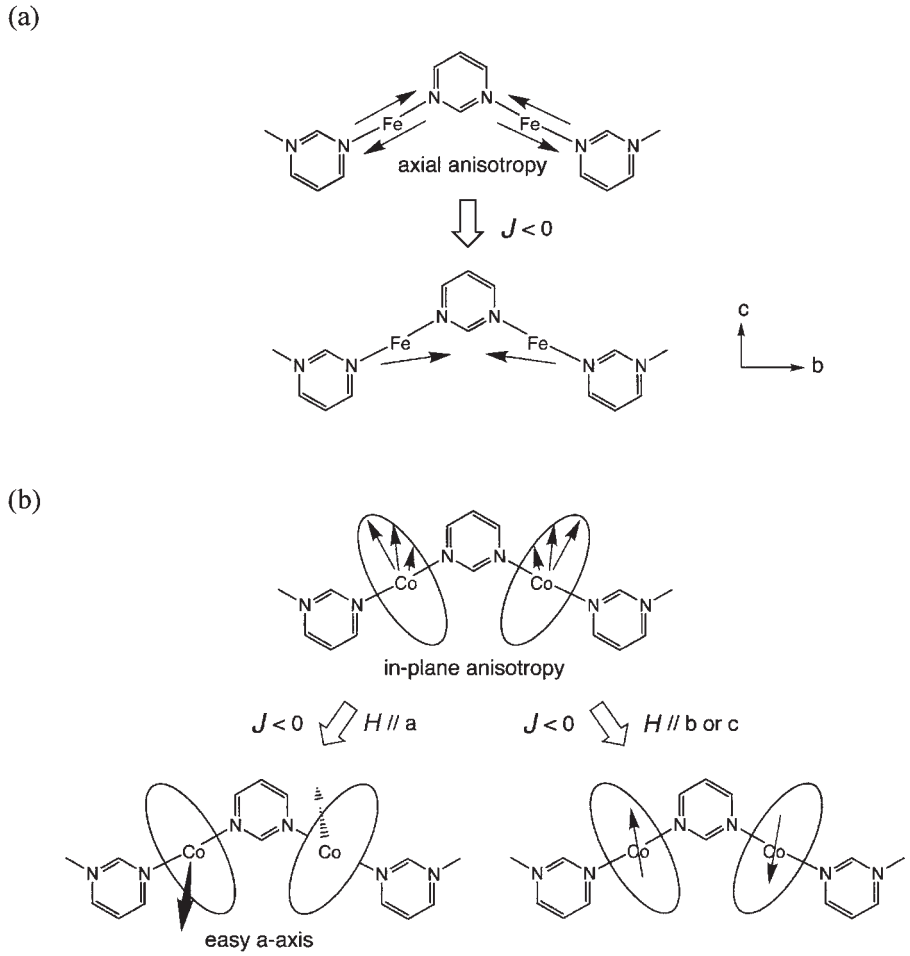

Fig. 9. Schematic drawings of the spin structures for **1** (a) and **5** (b).

tal results suggest the in-plane anisotropy of Fe^{II} in **2**, leading to the following conclusion: the guest molecule tunes the single-ion anisotropy of the host. Consequently, the magnetic phase transition phenomena were drastically different depending on the guest molecules.

The transition temperatures (T_N's) of **2**, **5**, and the nickel(II) analogue $[Ni\{N(CN)_2\}_2(pm)](H_2O)$[11] were 3.6, 2.0, and 8.3 K, respectively. We have reported another isomorphous series of $[MCl_2(pm)_2]$, whose T_N's are 6.1, 4.4, and 16 K for M = Fe,[17] Co,[18] and Ni,[17] respectively. Interestingly, the dependences of T_N upon metal ion species are parallel to each other. Furthermore, the transition temperatures of $[M\{N(CN)_2\}_2]$ (M = Fe: T_N = 18.5 K; M = Co: T_C = 9.2 K; M = Ni: T_C = 20.6 K)[6] show a similar tendency of the metal ion dependence. These findings support the conclusion that the transition phenomena are dominantly affected by the single ion properties. However, the proposed mechanism can only account for magnetic behavior within a pm-bridged zigzag chain. Problems about bulk residual moments surviving in a centrosymmetric crystal still remain.

Conclusion

Nano-porous materials generally tend to form interpenetrated structures, such as the nested rutile-like compounds,[6–8] or to include small guest molecules, as shown in the present study. In the latter case, we have a chance to control the physical properties of the host compounds by means of supramolecular techniques. We have shown that the solvated magnets $[M\{N(CN)_2\}_2(pm)](guest)$ are characterized as weak ferromagnts (canted antiferromagnets): **1** (M = Fe, guest = pm), T_N = 5.6 K, θ (cant angle) = 1.3° at 2 K with $H \parallel c$; **2** (M = Fe, guest = ethanol), T_N = 3.3 K, θ = 16° at 2 K with $H \parallel c$; **5** (M = Co, guest = ethanol), T_N = ca. 2 K, θ = 7.1° at 2 K with $H \parallel b$. The proposed mechanism of spin-canting based on the single-ion anisotropy is plausible. The S_z-character is suggested for the iron(II) ions in **1** for the definite anisotropic magnetization observed. On the other hand, the S_{xy}-character should be taken into consideration for the iron(II) ions in **2** and the cobalt(II) ions in **5** because the anisotropic magnetization measurements indicated that the spin could rotate according to the applied field. The magnetic phase transition phenomena were tuned by the guest molecules. The origin of the tuning is the variable single-ion anisotropy of the metal ions, which is susceptible to delicate coordination geometry changes.

Experimental

Preparation of Single Crystals. $[Fe\{N(CN)_2\}_2(pm)](pm)$ (1): An aqueous solution (6 mL) containing pm (0.11 g; 1.4 mmol) and $NaN(CN)_2$ (0.25 g; 2.8 mmol) was added to an aqueous solution (2 mL) containing $FeCl_2 \cdot 4H_2O$ (0.28 g; 1.4 mmol). The mixture was allowed to stand for a day at room temperature to give yellow single crystals of **1**. Elemental analysis, X-ray crystallo-

graphic analysis, and magnetic measurements of these compounds were done immediately after the isolation on a filter. In some cases practically colorless thin needles were obtained as a by-product; these were characterized as an isomeric one-dimensional compound $[Fe\{N(CN)_2\}_2(pm)_2]$.[22]

$[Fe\{N(CN)_2\}_2(pm)](EtOH)$ (2): Pm (0.080 g; 1.0 mmol) and $NaN(CN)_2$ (0.18 g; 2 mmol) were dissolved in a mixed solvent of ethanol (5 mL) and water (5 mL) and added to an aqueous solution (5 mL) containing $FeCl_2 \cdot 4H_2O$ (0.20 g; 1.0 mmol). The mixture was allowed to stand for a day at room temperature to give yellow single crystals of **2**. The single crystals of **3** and **4** were similarly prepared from *n*-PrOH–H_2O (1/4), and *n*-BuOH–H_2O (1/15) mixed solutions, respectively, by using pm/$NaN(CN)_2$/$FeCl_2$ with a ratio of 1/2/1.

$[Co\{N(CN)_2\}_2(pm)](EtOH)$ (5): Pm (0.080 g; 1.0 mmol) and $NaN(CN)_2$ (0.18 g; 2 mmol) were dissolved in a mixed solvent of ethanol (5 mL) and water (25 mL) and added to an aqueous solution (5 mL) containing $CoCl_2 \cdot 6H_2O$ (0.24 g; 1.0 mmol). The mixture was allowed to stand for two days at room temperature to give pink single crystals of **5**. The single crystals of **6** were similarly prepared from a *n*-PrOH–H_2O (1/10) mixed solvent.

Elemental Analysis. Elemental analysis (C,H,N) on a Fisons EA-1108 by a usual combustion method revealed that the composition formulae were $[Fe\{N(CN)_2\}_2(pm)](guest)$, where guest = pm, EtOH, *n*-PrOH, and $(n\text{-BuOH})_{1/2}$ for **1**–**4**, respectively, and $[Co\{N(CN)_2\}_2(pm)](guest)$ where guest = EtOH and *n*-PrOH for **5** and **6**, respectively. Anal. Calcd for **1**: C, 41.4; H, 2.3; N, 40.2%. Found: C, 40.6; H, 2.2; N, 40.8%. Calcd for **2**: C, 38.2; H, 3.2; N, 35.7%. Found: C, 38.6; H, 3.2; N, 36.6%. Calcd for **3**: C, 39.3; H, 3.4; N, 33.3%. Found: C, 40.3; H, 3.7; N, 34.2%. Calcd for **4**: C, 40.6; H, 3.4; N, 35.0%. Found: C, 39.4; H, 3.0; N, 36.7%. Calcd for **5**: C, 37.2; H, 3.4; N, 39.8%. Found: C, 37.5; H, 3.4; N, 39.9%. Calcd for **6**: C, 38.9; H, 3.3; N, 34.1%. Found: C, 39.9; H, 3.7; N, 33.8%.

X-ray Crystallographic Analysis. Diffraction data of single crystal of **1** were collected on a Rigaku R-axis RAPID diffractometer with graphite monochromated Mo Kα radiation ($\lambda = 0.71069$ Å) at 90 K. The structures were directly solved by a heavy-atom Patterson method in the teXsan program package.[23] Numerical absorption correction was used. All of the hydrogen atoms could be found in difference Fourier maps, and the parameters of the hydrogen atoms were included in the refinement. The thermal displacement parameters were refined anisotropically for non-hydrogen atoms and isotropically for hydrogen atoms. Full-matrix least-squares methods were applied using all of the unique diffraction data. The selected data for **1** are: $C_{12}H_8Fe_1N_{10}$, orthorhombic, *Pnma*, $a = 13.0061(5)$, $b = 12.3550(4)$, $c = 9.2235(4)$ Å, $V = 1482.1(1)$ Å^3, $Z = 4$, $D_{calc} = 1.560$ g cm^{-3}, $\mu = 1.033$ mm^{-1}, $R_1(I > 2\sigma(I)) = 0.0265$, and R_w(all data) = 0.0707, for 1771 diffractions ($2\theta \leq 55^\circ$) at $T = 90$ K. The crystallographic data of **1** in a cif format have been deposited with the CCDC (# 222024). The detailed results of the crystal structure analysis on **2** and **5** have been described elsewhere.[10] The analyses on **3** and **4** were also successful and their cell parameters were refined using all of the reflection data.

Magnetic Measurements. Dc and ac magnetic susceptibilities of polycrystalline samples of **1**–**6** were measured on Quantum Design MPMS SQUID and PPMS magnetometers equipped with 7 and 9 T coils, respectively, in a temperature range down to 1.8 K. The magnetic responses were corrected with diamagnetic blank data of the sample holder measured separately. The diamagnetic contribution of the sample itself was estimated from Pascal's constant. Ac magnetic susceptibilities were measured on a PPMS ac/dc magnetometer. An ac magnetic field (amplitude: 10 Oe, frequency: 100, 1000, and 10000 Hz) was applied to polycrystalline samples.

Single-crystal magnetization data of **1**, **2**, and **5** were obtained on the SQUID magnetometer. The sample was mounted inside on a probe tube with a slight amount of Apiezon H grease and the crystal axis was carefully oriented under a microscope. The crystal planes were defined with Miller indexes by means of X-ray diffraction, and the crystallographic axes could be assigned in a single crystal. The needle-like crystal was characterized with $(0\ \pm1\ 0)$ basal planes and $(\pm1\ 0\ \pm1)$ lateral faces. The sample mass was estimated from the sample dimensions and the density (D_{calc} in the X-ray diffraction study) and also from comparison of the magnetization averaged over the three axes with that of the randomly oriented polycrystalline sample.

This work was partly supported by a Grant-in-Aid for Scientific Research on Priority Areas of "Molecular Conductors" (No. 15073101) and by Grants-in-Aids for Scientific Research (Nos. 13640575 and 15550115), all from the Ministry of Education, Culture, Sports, Science and Technology.

References

1 P. J. Stang and B. Olenyuk, *Acc. Chem. Res.*, **30**, 502 (1997); O. M. Yaghi, H. Li, C. Davis, D. Richardson, and T. L. Groy, *Acc. Chem. Res.*, **31**, 474 (1998); M. Eddaoudi, D. B. Moler, H. Li, B. Chem, T. M. Reineke, M. O'Keeffe, and O. M. Yaghi, *Acc. Chem. Res.*, **34**, 319 (2001); S. Kitagawa and M. Kondo, *Bull. Chem. Soc. Jpn.*, **71**, 1739 (1998).

2 T. Ishida and T. Nogami, *Recent Res. Devel. Pure Appl. Chem.*, **1**, 1 (1997); T. Ishida, K. Nakayama, M. Nakagawa, W. Sato, Y. Ishikawa, M. Yasui, F. Iwasaki, and T. Nogami, *Synth. Met.*, **85**, 1655 (1997).

3 T. Ishida, L. Yang, and T. Nogami, *Chem. Lett.*, **32**, 1018 (2003), and references cited therein.

4 T. Ishida, S.-i. Mitsubori, T. Nogami, N. Takeda, M. Ishikawa, and H. Iwamura, *Inorg. Chem.*, **40**, 7059 (2001).

5 T. Ishida, T. Kawakami, S.-i. Mitsubori, T. Nogami, K. Yamaguchi, and H. Iwamura, *J. Chem. Soc., Dalton Trans.*, **2002**, 3177.

6 S. R. Batten, P. Jensen, B. Moubaraki, K. S. Murray, and R. Robson, *Chem. Commun.*, **1998**, 439; M. Kurmoo and C. J. Kepert, *New J. Chem.*, **22**, 1515 (1998); J. L. Manson, C. R. Kmety, Q. Z. Huang, J. W. Lynn, G. M. Bendele, S. Pagola, P. W. Stephens, L. M. Liable-Sands, A. L. Rheingold, A. J. Epstein, and J. S. Miller, *Chem. Mater.*, **10**, 2552 (1998); J. L. Manson, C. R. Kmety, A. J. Epstein, and J. S. Miller, *Inorg. Chem.*, **38**, 2552 (1999).

7 J. S. Miller and J. L. Manson, *Acc. Chem. Res.*, **34**, 563 (2001).

8 J. L. Manson, C. D. Incarvito, A. L. Rheingold, and J. S. Miller, *J. Chem. Soc., Dalton Trans.*, **1998**, 3705; J. L. Manson, Q.-Z. Huang, J. W. Lynn, H.-J. Koo, M.-H. Whangbo, R. Bateman, T. Otsuka, N. Wada, D. N. Argyriou, and J. S. Miller, *J. Am. Chem. Soc.*, **123**, 162 (2001).

9 P. Jensen, S. R. Batten, G. R. Fallon, D. C. R. Hockless, B. Moubaraki, K. S. Murray, and R. Robson, *J. Solid State Chem.*, **145**, 387 (1999).

10 T. Kusaka, T. Ishida, D. Hashizume, F. Iwasaki, and T. Nogami, *Chem. Lett.*, **2000**, 1146.

11 T. Kusaka, T. Ishida, D. Hashizume, F. Iwasaki, and T.

Nogami, *Mol. Cryst. Liq. Cryst.*, **376**, 463 (2002).

12 Y. Doi, T. Ishida, and T. Nogami, *Bull. Chem. Soc. Jpn.*, **75**, 2455 (2002); A. Escuer, R. Vicente, F. A. Mautner, M. A. S. Goher, and M. A. M. Abu-Youssef, *Chem. Commun.*, **2002**, 64.

13 E.-Q. Gao, A.-M. Wang, and C.-H. Yan, *Chem. Commun.*, **2003**, 1748; H.-L. Sun, B.-O. Ma, S. Gao, and G. Su, *Chem. Commun.*, **2001**, 2586.

14 A. Lappas, A. S. Wills, M. A. Green, K. Prassides, and M. Kurmoo, *Phys. Rev. B*, **67**, 4406 (2003).

15 For example, J. Omata, T. Ishida, D. Hashizume, F. Iwasaki, and T. Nogami, *Polyhedron*, **20**, 1557 (2001); T. Ishida, J. Omata, and T. Noagmi, *Polyhedron*, **22**, 2133 (2003).

16 T. Kusaka, T. Ishida, and T. Nogami, *Mol. Cryst. Liq. Cryst.*, **379**, 259 (2002).

17 R. Feyerherm, A. Loose, T. Ishida, T. Nogami, J. Kreitlow, D. Baabe, F. J. Litterst, S. Süllow, H.-H. Klauss, and K. Doll, *Phys. Rev. B*, in press; K. Zusai, T. Kusaka, T. Ishida, R. Feyerherm, M. Steiner, and T. Nogami, *Mol. Cryst. Liq. Cryst.*, **343**, 127 (2000).

18 K. Nakayama, T. Ishida, R. Takayama, D. Hashizume, M. Yasui, F. Iwasaki, and T. Nogami, *Chem. Lett.*, **1998**, 497.

19 T. Yuen, C. L. Lin, A. Fu, and J. Li, *J. Appl. Phys.*, **91**, 7385 (2002); A. Fu, X. Huang, J. Li, T. Yuen, and C. L. Lin, *Chem.—Eur. J.*, **8**, 2239 (2002).

20 J.-S. Sun, H. Zhao, X. Ouyang, R. Clérac, J. A. Smith, J. M. Clemente-Juan, C. Gómez-Garcia, E. Coronado, and K. Dunbar, *Inorg. Chem.*, **38**, 5841 (1999).

21 E.-C. Yang, D. N. Hendrickson, W. Wernsdorfer, M. Nakano, R. Sommer, A. L. Rheingold, M. Ledezma-Gairaud, and G. Christou, *J. Appl. Phys.*, **91**, 7382 (2002); J.-P. Costes, F. Dahan, and J. Garcia-Tojal, *Chem.—Eur. J.*, **8**, 5430 (2002).

22 The cell constants of $[Fe\{N(CN)_2\}_2(pm)_2]$: triclinic, $P\bar{1}$, $a = 6.238(1)$, $b = 7.400(2)$, $c = 9.0999(9)$ Å, $\alpha = 109.16(2)$, $\beta = 105.82(1)$, and $\gamma = 90.22(2)^\circ$ at $T = 100$ K. A preliminary analysis indicates that the Fe^{II} ions are doubly bridged with $N(CN)_2^-$ anions in a μ-1,5 manner to form a one-dimensional structure and that both pms do not work as a bridge but as a monodentate pendant.

23 teXsan: crystal structure analysis package, Molecular Structure Corp., The Woodlands, TX, 1985, 1999.